Single-nanotube tracking reveals the nanoscale organization of the extracellular space in the live brain

Antoine G. Godin, Juan A. Varela, Zhenghong Gao, Noémie Danné, Julien P. Dupuis, Brahim Lounis, Laurent Groc, Laurent Cognet

Title : Single nanotube tracking reveals the extracellular space nanoscale organization in live brain tissue

Antoine G. Godin[1,2,*], Juan A. Varela[3,4,*], Zhenghong Gao[1,2,*], Noémie Danné[1,2], Julien P. Dupuis[3,4], Brahim Lounis[1,2], Laurent Groc[3,4] and Laurent Cognet[1,2]

Affiliations

[1]Univ. Bordeaux, Laboratoire Photonique Numérique et Nanosciences, UMR 5298, F-33400 Talence, France

[2]Institut d'Optique & CNRS, LP2N UMR 5298, F-33400 Talence, France

[3]Univ. Bordeaux, Interdisciplinary Institute for Neuroscience, UMR 5297, F-33000 Bordeaux, France

[4]CNRS, IINS UMR 5297, F-33000 Bordeaux, France

*These authors contributed equally to this work.

The brain is a dynamic structure in which the extracellular space (ECS) takes up almost a quarter of its volume[1-2]. Signalling molecules, neurotransmitters and nutrients transit *via* the ECS which constitutes a key microenvironment for cellular communication[3] and clearance of toxic metabolites. The ECS spatial organization varies during sleep[4], development[5], aging[6] and is likely altered in neuropsychiatric and degenerative diseases[7], as inferred from electron microscopy[8-9] and macroscopic biophysical investigations[2,10]. Here we show an approach to directly observe the local ECS structures and rheology in a brain tissue using super-resolution imaging. We inject single-walled carbon nanotubes (SWCNTs) in rat cerebroventricles and follow individual nanotubes near-IR emission for tens of minutes in acute slices as they diffuse inside the ECS. Because of the interplay between the nanotube geometry and the ECS local environment, we can extract information about the ECS dimension and local viscosity. We find a striking diversity of ECS dimensions down to 40 nm, and as well as of local viscosity values. Moreover, by

chemically altering the brain extracellular matrix of the live animals before nanotube injection, we reveal that ECS rheology properties are affected, but that ECS alterations are local and inhomogeneous at nanoscale dimensions.

Investigations of the fine structure of live brain ECS require brain preparations that best preserve cellular architectures. In that respect, we used acute brain slices as opposed to other preparations that poorly preserve native tissue organization, e.g. cultured neurons or organotypic slices. Moreover, one needs an imaging modality reaching spatial resolutions beyond the diffraction limit as well as tissue access deeper than the first 2-3 pyramidal cell layers inside the slice (> ~30µm) to avoid regions affected during slicing. To this aim, deep tissue localization microscopy based on tracking the successive positions of single nano-emitters while they explore brain tissues would represent a unique approach.

Near-infrared luminescent SWCNTs were previously proposed as unique probes for ensemble imaging in whole animal[11-12] due to their brightness, photostability and spectral imaging range[13-14], as well as for intracellular single molecule tracking in cultured cells[15-16]. It was also shown, at the ensemble level, that their unusual length-to-diameter aspect ratios contribute to enhance their penetration within multicellular tumour spheroids depending on the encapsulation agents used[17-18]. In fact, in contrast to spherical nanoparticles, SWCNTs have two characteristic dimensions impacting their diffusion behaviours. Their small diameter (nanometer scale) confers them a remarkable accessibility in complex environments, while the combination of their length and rigidity can moderate their diffusion rates so as to be compatible with video-rate single molecule imaging[19].

SWCNTs were delivered into young rat brains by injection of a small volume (5 µl, 3 µg/mL) of solubilized nanotubes in the lateral cerebroventricles (Figure 1a) [20]. This SWCNT delivery method generates minimal tissue inflammation as the gross morphology and density of microglial cells – the resident macrophages of the brain- were found to be similar in buffer- and SWCNT-injected brains (Figure S1). SWCNTs coated with phospholipid-polyethylene glycol (PL-PEG) were used since they display low cytotoxicity as compared to other encapsulation methods of luminescent SWCNTs[21-22]. Rats were sacrificed 30 min after the ventricular injection and acute brain slices were prepared for observation under a wide field fluorescent NIR microscope (Figure 1b). Wavelengths of excitation (845 nm to excite (6,5) SWCNTs at a phonon

sideband[23]) and emission (986 nm for (6,5) SWCNTs) are in the transparency window of the studied brain tissues (Figure 1c) and as such, minimize tissue phototoxicity (Figures S2 and S3). Phonon sideband excitation also ensures better emission photostability[23] as compared to high photon-energy excitation commonly used to excite SWCNT at their second order electronic transition (Figure S4).

Single luminescent (6,5) SWCNTs were detected in diverse areas of sagittal brain slices (*e.g.* neocortex, hippocampus, striatum) (Figure S5). Imaging was performed at different depths in the brain slices, from a few tens of μm to avoid the damaged superficial layers up to ~100 μm (Figure S6). The broad SWCNT dissemination away from cerebroventricular injection site was surely facilitated by their nanometer-size diameters, and also suggests that SWCNTs were primarily located in the ECS since such a large dissemination would not be possible if SWCNTs were internalized in brain cells. The diffusion of molecules in the ECS is thought to be globally governed by several parameters such as the geometric path length, trapping in dead space domains, and ECS viscosity by molecular crowding and transient molecular interactions. At a macroscopic scale, these parameters participate to the so-called tortuosity of the ECS[2,24]. Many SWCNTs were found immobilized away from the ventricular injection zones, likely originating from non-specific interactions with molecules of the ECS (although PL-PEG coating minimizes this effect in live cell culture (Figure S7) and live animals[21]), and/or by the existence of dead-space microdomains[2]. The direct observation of PL-PEG-coated SWCNT trapping is thus consistent with the existence dead-space domains in the ECS. To further ascertain extracellular location, we directly loaded SWCNTs within hippocampal pyramidal neurons through a patch-clamp pipette. The behaviours of detected intracellular SWCNTs were distinct from cerebroventricular injected ones (Figure S8), further supporting that SWNCTs imaged after icv injection are primarily extracellular.

The movements of individual SWCNTs exploring the ECS could be resolved with video rate fluorescence imaging (Figure 1d). This is primarily due to the SWCNT high aspect-ratio and rigidity, linked to their nanometer diameter, which significantly slows down their diffusion in the ECS maze, as compared to nanometer sized probes or fully flexible polymers. We indeed checked that small isotropic fluorescent probes diffuse too fast in the ECS to be imaged at video rate for a long time (observed trajectories < 1s, Figure S9). In addition, we could record long movies of single SWCNT (x, y) diffusion occurring during more than 20,000 frames within the

~1µm depth-of-focus of the microscope (Movie 1). By means of two-dimensional asymmetric Gaussian fitting analysis, we extracted in each movie frame i the nanotube center-of-mass localization (x_i, y_i) in the imaging plane with sub-wavelength precision (~ 40 nm) and its axis orientation θ_i relative to the x axis in the laboratory frame (Figure 1c, inset). Analysis of the fitted 2D Gaussian asymmetry provides a measure of the nanotube lengths L which range here from ~490-780 nm. These lengths match the typical SWCNT lengths of the injected solution determined by AFM imaging (Figure S10). Assuming characteristic ECS dimensions ξ larger than 50 nm, these SWCNTs behave as rigid rods in the ECS and their diffusion should be independent of flexibility[19]. The nanotube movements along ($\parallel$) and perpendicular ($\perp$) to their axis were then decoupled to calculate two 1D Mean Squared Displacements $MSD_{\parallel}$ and $MSD_{\perp}$ as a function of time (Figure 2a). The MSD_{xy} corresponding to the 2D movements in the laboratory frame was also calculated. On short time scales ($t < t_c \sim 200\, ms$), MSD_{xy} is linear with time and $MSD_{xy} \sim MSD_{\parallel} + MSD_{\perp}$ while for longer times MSD_{xy} levels off and $MSD_{\parallel} + MSD_{\perp}$ is close to linear, such that $MSD_{xy} < MSD_{\parallel} + MSD_{\perp}$ (Figure 2a). The different behaviours of MSD_{xy} and $MSD_{\parallel} + MSD_{\perp}$ indicates that nanotube movements are not free[25] and thus constrained by local ECS environment. The deviation from linearity of MSD_{xy} also suggests that t_c represents a characteristic time scale during which SWCNTs explore single ECS sub-domains.

Because MSDs calculated on full trajectories inherently reflect average displacements, the properties of transient diffusive states can hardly be retrieved by the direct analysis of MSD_{xy}, $MSD_{\parallel}$ or $MSD_{\perp}$. To access transient diffusive states in local environments, we used instead an analytical analysis based on the Distribution of Squared Displacements (DSD)[26-27] along and perpendicular to the nanotube axis $DSD_{\tau}(r^2_{\parallel,\perp})$ defined for different time lags τ with $\tau < t_c$ (supplemental materials). Along each direction ($\parallel, \perp$), two diffusion behaviors are found characterized by the time dependence of their mean $MSDs$ denoted $\langle \mathrm{r}_{\parallel,\perp}{}^2 \rangle_j(\tau)$, where $j = 1$ corresponds to the slowest SWCNT diffusive states and $j = 2$ to faster ones (Figure S11). The population of small displacements perpendicular to SWCNT axis is bounded as evidenced by the fast saturation of $\langle \mathrm{r}_{\perp}{}^2 \rangle_1(\tau)$ (Figure 2b) while other states display mainly unrestricted diffusion (Figure 2b and S11). This behaviour can be related to successive diffusion episodes occurring in different ECS confinement domains (see below). The plateau of $\langle \mathrm{r}_{\perp}{}^2 \rangle_1(\tau)$, which equals $\langle \xi \rangle^2/6$ for confined diffusion along a 1D coordinate[28], provides a

measure of $\langle\xi\rangle$ representing the average confining ECS dimension (Figure 2b). As displayed in Figure 2c, $\langle\xi\rangle$ ranges from 80 to 270 nm (150 ± 40 nm, mean ± SD). This dynamic analysis demonstrates that anisotropic diffusion behaviours of single SWCNTs locally probe the brain ECS and can reveal nanoscale dimensions (Figure 2d).

Using a similar approach as in single-molecule localization microscopy[29], a large number of nanotube localization coordinates obtained with sub-diffraction precisions were pooled to create a super-resolved image of the ECS (Figure 3a). Such images directly unveil the spatial, nanoscale and structural tortuosity of the live brain ECS. The ECS maze is heterogeneous and consists of many connected submicron structural domains of various sizes. A total of 419 ECS domains were identified with typical dimensions ξ ranging from ~ 50 to 700 nm (Figure 3b and S12). Noteworthy, the ECS nanoscale dimensions and morphologies described here in live brain samples resembles the ECS morphology visualized by electron microscopy following cryo-fixation of brain tissues[8-9] (Figure S13). Maps of the instantaneous diffusion constants calculated along nanotube trajectories on 300 ms sliding time windows were constructed (Figure 3c) to evaluate the spatial dependence of the local SWCNT diffusion in live brain tissue. From the knowledge of nanotube lengths, high-resolution spatial maps of the ECS viscosity were also obtained (Figure 3c and Extended Data Movie 1). Viscosity values ranged from ~ 1 to 50 mPa·s which is up to two orders of magnitude larger than that of the cerebrospinal fluid. These viscosity maps reveal that ECS local viscosity is spatially inhomogeneous. Interestingly, within this viscosity range, the instantaneous diffusion constants of quantum dots in the ECS, having hydrodynamic diameters of 35 nm would locally vary from ~ 0.1 to 10 $\mu m^2 s^{-1}$. As expected, the average diffusion constant of such quantum dots (~ 0.1 $\mu m^2 s^{-1}$) previously observed on macroscopic spatial scales in the ECS[24] is constrained towards the smallest local values and cannot divulge the diversity of local viscosities. By comparing Figures 3a&c, the spatial dependence of the ECS rheological properties indicates that locally ECS viscosity values do not correlate with ECS dimensions. Indeed, although ξ values span up to two orders of magnitude, SWCNT instantaneous diffusion constants vary over up to three decades independently of the ECS dimensions in which SWCNTs are diffusing. Although bearing diffusion properties not necessarily identical to those of endogenous molecules diffusing in the brain ECS, our findings demonstrate that SWCNT tracking unveils and quantifies the diversity of nanoscale diffusive environments composing the ECS. Interestingly, considering the ECS as a fluidic connected

space with specialized functional regions[2,4], our results indicate that local structural dimensions are not sole responsible for affecting molecular diffusion properties of the ECS. It follows that other mechanisms including fine-tuned molecular interactions involving constitutive components of the ECS must play an important role for controlling local diffusion of e.g. endogenous signalling molecules or nutrients in local areas of interest.

In order to support this hypothesis, we then biochemically altered the ECS structure by injecting hyaluronidase in the brain lateral ventricles of young rats several hours before nanotube injection and imaging, a time period supposedly sufficient to significantly digest hyaluronic acid[30]. We first confirmed alterations of the ECM components in hyaluronidase-injected brains as attested by strong decrease of both hyaluronan binding protein (HABP) (Figures 4a-d) and aggrecan immunostaining (Extended Figure 14). Noteworthy, we did not observe modification of the morphology of neuronal soma and overall cellular density in hyaluronidase-injected brains at spinning-disk confocal resolution. Analysis of SWCNT diffusion indicates that they explored wider areas as compared to naive brains within identical time scales (Figures 4e&f). Consistent with hyaluronidase-induced disappearance of ECM components, instantaneous diffusion coefficients were significantly increased (calculated as in Figure 3b), indicating a global reduction of medium viscosity (Figures 4g&h, Movie 2). More precisely, the histogram of diffusion coefficients from naive brains was well fitted by a single lognormal distribution whereas in the altered brains two lognormal distributions were needed, with one of them being indistinguishable from the one used to fit the histogram of naive brains (Figure 4h). This demonstrates that hyaluronidase effect is in fact not spatially homogeneous in the ECS (see also Figure 4g). Characterizing the ECS dimensions explored by SWCNTs using the DSD analysis, a moderate but significant reduction of mean size values $\langle \xi \rangle$ was found in altered brain (280 ± 60 nm) as compared to naive ones (150 ± 40 nm) (Figure 4i). This indicates that upon profound but non-uniform alteration of the ECM, the ECS topology offers larger territories for SWCNT nanoscale molecular exploration.

Here, we provide a new approach to reveal the ECS dimensions and viscosity at the nanoscale in live brain tissue of young rats. The ECS appears as a maze of interconnected polymorphic compartments structured down to the nanoscale and bearing specific rheological properties. This knowledge will surely influence our understanding of the chemical-based

cellular communication in brain physiology and pathology. In addition, detailed knowledge of nanoscale ECS network should also foster new drug delivery strategies.

References

1 Cserr, H. F. *et al.* Extracellular volume decreases while cell-volume is maintained by ion uptake in rat-brain during acute hypernatremia. *J. Physiol.-London* **442**, 277-295 (1991).

2 Sykova, E. & Nicholson, C. Diffusion in brain extracellular space. *Physiol. Rev.* **88**, 1277-1340 (2008).

3 Dityatev, A., Schachner, M. & Sonderegger, P. The dual role of the extracellular matrix in synaptic plasticity and homeostasis. *Nat. Rev. Neurosci.* **11**, 735-746 (2010).

4 Xie, L. *et al.* Sleep drives metabolite clearance from the adult brain. *Science* **342**, 373-377 (2013).

5 Lehmenkuhler, A., Sykova, E., Svoboda, J., Zilles, K. & Nicholson, C. Extracellular space parameters in the rat neocortex and subcortical white matter during postnatal development determined by diffusion analysis. *Neuroscience* **55**, 339-351 (1993).

6 Metzler-Baddeley, C., Jones, D. K., Belaroussi, B., Aggleton, J. P. & O'Sullivan, M. J. Frontotemporal connections in episodic memory and aging: a diffusion MRI tractography study. *J. Neurosci.* **31**, 13236-13245 (2011).

7 Berezin, V., Walmod, P. S., Filippov, M. & Dityatev, A. Targeting of ECM molecules and their metabolizing enzymes and receptors for the treatment of CNS diseases. *Prog. Brain Res.* **214**, 353-388 (2014).

8 Ohno, N., Terada, N., Saitoh, S. & Ohno, S. Extracellular space in mouse cerebellar cortex revealed by in vivo cryotechnique. *J. Comp. Neurol.* **505**, 292-301 (2007).

9 Korogod, N., Petersen, C. C. & Knott, G. W. Ultrastructural analysis of adult mouse neocortex comparing aldehyde perfusion with cryo fixation. *Elife* **4** (2015).

10 Verkman, A. S. Diffusion in the extracellular space in brain and tumors. *Phys. Biol.* **10**, 045003 (2013).

11 Welsher, K. *et al.* A route to brightly fluorescent carbon nanotubes for near-infrared imaging in mice. *Nat. Nanotechnol.* **4**, 773-780 (2009).

12 Heller, D. A. *et al.* Multimodal optical sensing and analyte specificity using single-walled carbon nanotubes. *Nat. Nanotechnol.* **4**, 114-120 (2009).

13 Bachilo, S. M. *et al.* Structure-assigned optical spectra of single-walled carbon nanotubes. *Science* **298**, 2361-2366 (2002).

14 Cognet, L. *et al.* Stepwise quenching of exciton fluorescence in carbon nanotubes by single-molecule reactions. *Science* **316**, 1465-1468 (2007).

15 Reuel, N. F., Dupont, A., Thouvenin, O., Lamb, D. C. & Strano, M. S. Three-dimensional tracking of carbon nanotubes within living cells. *ACS Nano* **6**, 5420-5428 (2012).

16 Fakhri, N. *et al.* High-resolution mapping of intracellular fluctuations using carbon nanotubes. *Science* **344**, 1031-1035 (2014).

17 Wang, Y., Bahng, J. H., Che, Q., Han, J. & Kotov, N. A. Anomalously Fast Diffusion of Targeted Carbon Nanotubes in Cellular Spheroids. *ACS Nano* **9**, 8231-8238 (2015).

18 Jena, P. V. *et al.* Photoluminescent carbon nanotubes interrogate the permeability of multicellular tumor spheroids. *Carbon N Y* **97**, 99-109 (2016).

19 Fakhri, N., MacKintosh, F. C., Lounis, B., Cognet, L. & Pasquali, M. Brownian motion of stiff filaments in a crowded environment. *Science* **330**, 1804-1807 (2010).

20 Varela, J. A. *et al.* Targeting neurotransmitter receptors with nanoparticles in vivo allows single-molecule tracking in acute brain slices. *Nat Commun* **7**, 10947 (2016).

21 Liu, Z. *et al.* In vivo biodistribution and highly efficient tumour targeting of carbon nanotubes in mice. *Nat. Nanotechnol.* **2**, 47-52 (2007).

22 Gao, Z., Varela, J. A., Groc, L., Lounis, B. & Cognet, L. Toward the suppression of cellular toxicity from single-walled carbon nanotubes. *Biomater. Sci.* **4**, 230-244 (2016).

23 Santos, S. M. *et al.* All-optical trion generation in single-walled carbon nanotubes. *Phys. Rev. Lett.* **107**, 187401 (2011).

24 Thorne, R. G. & Nicholson, C. In vivo diffusion analysis with quantum dots and dextrans predicts the width of brain extracellular space. *Proc. Natl. Acad. Sci. U.S.A.* **103**, 5567-5572 (2006).

25 Han, Y. *et al.* Brownian motion of an ellipsoid. *Science* **314**, 626-630 (2006).

26 Schutz, G. J., Schindler, H. & Schmidt, T. Single-molecule microscopy on model membranes reveals anomalous diffusion. *Biophys. J.* **73**, 1073-1080 (1997).

27 Tardin, C., Cognet, L., Bats, C., Lounis, B. & Choquet, D. Direct imaging of lateral movements of AMPA receptors inside synapses. *EMBO J.* **22**, 4656-4665 (2003).

28 Kusumi, A., Sako, Y. & Yamamoto, M. Confined lateral diffusion of membrane receptors as studied by single particle tracking (nanovid microscopy). Effects of calcium-induced differentiation in cultured epithelial cells. *Biophys. J.* **65**, 2021-2040 (1993).

29 Godin, A. G., Lounis, B. & Cognet, L. Super-resolution microscopy approaches for live cell imaging. *Biophys. J.* **107**, 1777-1784 (2014).

30 Kochlamazashvili, G. *et al.* The extracellular matrix molecule hyaluronic acid regulates hippocampal synaptic plasticity by modulating postsynaptic L-type Ca(2+) channels. *Neuron* **67**, 116-128 (2010).

Ackowledgements. We warmly thank E. Bézard, M. Blanchard-Desce, B. Bontempi and P. Bon for helpful discussions. We thank J.P. Salvetat for experimental help for AFM imaging, and J. Ferreira for support with histological experiments. This work was supported by CNRS, Agence Nationale de la Recherche (ANR-14-OHRI-0001-01), IdEx Bordeaux (ANR-10-IDEX-03-02), Labex Brain (ANR-10-LABX-43), Conseil Régional d'Aquitaine (2011-1603009) and the France-BioImaging national infrastructure (ANR-10-INBS-04-01). A.G.G. acknowledges financial support from the Fondation pour la Recherche Médicale and the Fonds Recherche du Québec – Nature et Technologies. J.A.V. acknowledges Marie Curie Individual Fellowship 326442 funding.

Author contributions statement. A.G.G., J.A.V., Z.G. and J.P.D. performed the experiments. A.G.G., N.D., B.L. and L.C. performed the analysis. B.L., L.G. and L.C. co-supervised the study. L.G. and L.C. designed the study. All authors discussed the results and co-wrote the manuscript.

Competing financial interest statement. We declare no competing financial interests.

Additional information. Supplementary information is available in the online version of the paper. Reprints and permission information is available online at www.nature.com/reprints. Correspondence and requests for materials should be addressed to L.C. (laurent.cognet@u-bordeaux.fr) & L.G. (laurent.groc@u-bordeaux.fr). Analysis codes used in this study are available upon request to L.C. or L.G.

Figure caption

Figure 1. Single molecule tracking of luminescent SWCNTs in live ECS brain tissue. (**a**) SWCNTs are injected in lateral ventricles of living rats and diffuse into the neocortex. (**b**) Luminescent SWCNTs are imaged in brain slices. (**c**) Absorbance spectrum of 1 mm thick brain slice (black) and photoluminescence spectrum of a single (6,5) SWCNT in the ECS (red) upon 845 nm laser excitation (purple). (**c, inset**) Photoluminescence image of a (6,5) SWCNT recorded in the ECS with its orientation $\boldsymbol{\theta}$. (**d**) Color-coded trajectory of a single SWCNT diffusing in live ECS (20,000 data points). Scale bars = 1 **µ**m.

Figure 2. SWCNT diffusion properties in the ECS. (a) $\mathbf{MSD_{x,y}}(\boldsymbol{\tau})$ in the laboratory frame (black squares) and $\mathbf{MSD}_{\parallel,\perp}(\boldsymbol{\tau})$ calculated along (blue circles) and perpendicular (red diamonds) to the SWCNT axis for a 2D trajectory recorded in the ECS. Purple crosses correspond to $\mathbf{MSD}_{\parallel} + \mathbf{MSD}_{\perp}$. (**b**) Evolution of the mean MSDs for the slow diffusion states $\langle \mathbf{r}_{\parallel,\perp}{}^{\mathbf{2}} \rangle_{\mathbf{1}}(\boldsymbol{\tau})$ retrieved from the analysis of the DSDs. The plateau of $\langle \mathbf{r}_{\perp}{}^{\mathbf{2}} \rangle_{\mathbf{1}}(\boldsymbol{\tau})$ gives an average ECS domain size $\langle \boldsymbol{\xi} \rangle$ of 160 nm. (**c**) Histograms of $\langle \xi \rangle$ values measured from all single SWCNT trajectories as in (b). (**d**) Schematic representation of a SWCNT diffusing in the ECS.

Figure 3. Super-resolution imaging of ECS morphology and ECS local viscosity maps. (**a**) Super-resolved image of live brain ECS morphology obtained from 20,000 localizations of a diffusing SWCNT. Scale bar = 500 nm. (**b**) Histogram of ECS domain dimensions ξ (N = 419) from 14 ECS super-resolved images as in (a). (**c**) Spatial map of SWCNT instantaneous diffusion coefficients calculated along the same trajectory using a sliding window of 300 ms. This representation also constitutes a high-resolution spatial map of ECS viscosities (see scale bar).

Figure 4. ECS local modifications in chemically altered brains. Representative images of HAPB immunostaining in brain slices from naïve (**a**) and hyaluronidase-injected rats (altered, **b**). Neuronal nuclei are labelled with DAPI (blue). Scale bar: 250 μm. High magnification spinning disk microscope images of HAPB staining in both conditions are also presented (**c**, **d**). Scale bar: 20 μm. (**e**) Examples of super-resolved ECS images of naive *vs.* altered live brain tissues. Scale bars: 2 μm. (**f**) Areas explored normalized by SWCNT trajectory lengths. (**g**) Corresponding spatial viscosity maps. (**h**) Histograms of all instantaneous diffusion coefficients. In naive brains, the distribution is fitted with a single log-normal distribution (0.08±0.08 µm^2/s, median±s.d.)

while in altered brains, two independent log-normal distributions are needed (0.09±0.11 $\mu m^2/s$ & 0.28±0.26 $\mu m^2/s$). (**i**) Average ECS domain dimensions $\langle \xi \rangle$ as in Figure 2e for the two conditions. Statistical tests are two-tailed unpaired Mann-Whitney t-test ** $p<0.01$.

Methods

SWCNT preparation. PL-PEG preparation. HiPco synthesized nanotubes (batch no. 195.7 bought from Rice University) were suspended by biocompatible phospholipid-polyethylene glycol (PL-PEG) molecules (#MPEG-DSPE-5000, Laysan Bio, Inc.) which prevent nonspecific biomolecules absorption, minimize nanotubes sticking, and allow nanotubes diffusion in live tissue[1-2]: 2 mg of raw SWCNTs and 100 mg PL-PEG were added in 2 ml Milli-Q water and dispersed by tip sonication (6W output for 3 minutes). Nanotubes bundles and impurities were precipitated by centrifuging the dispersion at 10,000 rpm for 60 min at 4°C. The supernatant was collected and stored at 4°C for brain injection within 48 hours. The concentration of PL-PEG SWCNT solution was estimated to 3 μg/ml. From the two-dimensional photoluminescence excitation/emission map of the injected SWCNT solution (Figure S15), the subpopulation of (6,5) SWCNTs is estimated to represent 3-5% of the total population, such that SWCNTs detected in the brain slices at low density, are not affected by other chiralities. PL-PEG-NH_2 preparation: SWCNT were also suspended by biocompatible phospholipid-polyethylene glycol-amine (PL-PEG-NH_2) molecules (#MPEG-DSPE-NH_2-5000, Laysan Bio, Inc.) : 1 mg of raw SWCNTs and 15 mg PL-PEG-NH_2 were added in 1 mL Milli-Q water and 0.5 ml Deuterium Oxide and dispersed by tip sonication (8 W output for 30 seconds). Nanotubes bundles and impurities were precipitated by centrifuging the dispersion at 10,000 rpm for 45 min at 4 °C. The supernatant was collected and stored at 4 °C for experiments (0.4 μg/mL).

Intraventricular injections. Sprague-Dawley rats (Janvier, France) were used for this work, both male and female, treated according to the guidelines of the University of Bordeaux/CNRS Animal Care and Use Committee. Injections of SWCNTs were performed in living Sprague-Dawley rat pups (1-4 days old) anesthetized by hypothermia. Approximately 5 μl of SWCNTs dispersion were injected in each lateral ventricle (12 rats). Under cold light illumination, the injection place was found by firstly drawing a virtual line between the eye and lambda (easily seen through the skin), secondly finding the midpoint of that line, and thirdly moving 2 mm

caudal from that mid-point along the virtual line. The injection was performed in that point, at a depth of 2.6 mm for P1 pups, 2.9 mm for P2 pups, 3.1 mm for P3 pups and 3.5 mm for P4 pups. For hyaluronidase studies the intraventricular injection was performed in the same way (3 rats), injecting hyaluronidase from bovine testes 20 mg/mL in PBS (Sigma Aldrich #H3506) the night before injecting SWCNT.

Acute brain slices preparation. Between 10 min and up to 3 h after SWCNT injection, pups were decapitated and parasagittal brain slices (0.5 mm thick) were prepared in an ice-cold artificial cerebrospinal fluid (ACSF) solution containing (in mM): 126 NaCl, 3.5 KCl, 2 $CaCl_2$, 1.3 $MgCl_2$, 1.2 NaH_2PO_4, 25 $NaHCO_3$, and 12.1 glucose (gassed with 95% O_2 / 5% CO_2; pH 7.35). Slices were then imaged in oxygenated ACSF at 33°C perfused in the imaging chamber with a peristaltic pump.

Immunostainings. Staining of Iba1, Aggrecan and HABP were performed in coronal brain slices of 80 µm thickness. Before antibody incubation, slices were incubated with PBS-Triton-X100 1% and 4% BSA for 2h under agitation at room temperature. Slices were subsequently washed three times with PBS for 5 min each time. Slices were incubated overnight at 4 °C with primary antibodies in PBS-Triton-X100 0.2% and 2% BSA solution. Anti-Iba1 rabbit antibody (Wako Pure Chemical Industries #019-19741) was used at a 1:200 dilution. Anti-Aggrecan rabbit antibody (Millipore #AB1031) was used at a 1:200 dilution. Biotinilated HABP (Amsbio #AMS.HKD-BC41) was also used at a 1:200 dilution. Slices were subsequently washed three times with PBS for 5 min each time, and incubated with secondary reagents. Anti-Iba1 and anti-Aggrecan antibodies were labelled with goat anti-rabbit Alexa568 (ThermoFisher Scientific #A-11011) in PBS-Triton-X100 0.2% and 2% BSA solution for 2h at room temperature under agitation, at a 1:1000 dilution. Biotinilated HABP was labelled with Alexa568 streptavidin (ThermoFisher Scientific #S11226) in PBS-Triton-X100 0.2% and 2% BSA solution for 2h at room temperature under agitation, at a 1:1000 dilution. Slices were finally washed three times with PBS and mounted in glass slides with Vectashield+DAPI (Vector Labs).

Organotypic slice preparation. Organotypic slice cultures were prepared as previously described[3]. Briefly, 350 µm thick hippocampal slices were obtained from postnatal day 5 to

postnatal day 7 Sprague-Dawley rats using a McIlwain tissue chopper, and were placed in a pre-heated (37°C) dissection medium containing (in mM): 175 sucrose, 25 D-glucose, 50 NaCl, 0.5 $CaCl_2$, 2.5 KCl, 0.66 KH_2PO_4, 2 $MgCl_2$, 0.28 $MgSO_4$-$7H_2O$, 0.85 Na_2HPO_4-$12H_2O$, 2.7 $NaHCO_3$, 0.4 HEPES, 2 x 10-5 % phenol red, pH 7.3 (all products from Sigma unless specified). After 25 min of incubation, slices were transferred on white FHLC membranes (0.45 µm) set on Millicell Cell Culture Inserts (Millipore, 0.4 mm; Ø 30 mm), and cultured for up to 14 days on multiwell-plates at 35°C / 5% CO_2 in a culture medium composed of 50 % Basal Medium Eagle, 25 % Hank's balanced salt solution 1X (with $MgCl_2$ / with $CaCl_2$), 25 % heat-inactivated horse serum, 0.45 % D-glucose, 1 mM L-glutamine (all products from Gibco unless specified). The medium was changed every 2-3 days.

Single cell electroporation. Electroporation of single pyramidal neurons was performed as previously described[4]. Briefly, individual CA1 pyramidal neurons from 4-6 days in vitro hippocampal slices were electroporated to transfect cDNA encoding EGFP. Plasmids (5 µl at 1 µg/µl) were dissolved in a filtered cesium-based solution containing (in mM): 135 cesium-methanesulfonate, 8 NaCl, 10 HEPES, 0.2 EGTA, 4 Na_2ATP, 0.33 Na_3GTP, 5 tetraethylammonium chloride, pH 7.3 (all products from Sigma unless specified). This solution was supplemented with 10 µL of filtered endotoxin-free buffer TE (Qiagen), then centrifuged twice to pull down potential debris (10000 rpm, 15 min, 4°C) and used to fill 5-6 MΩ borosilicate patch pipettes. Electroporation was performed in 2 mL of pre-warmed (37°C / 5% CO_2) HEPES-based artificial cerebrospinal fluid (ACSF) containing (in mM): 130 NaCl, 2.5 KCl, 2.2 $CaCl_2$, 1.5 $MgCl_2$, 10 HEPES, 10 D-glucose. Plasmid transfer was allowed by the delivery of 50 µs-width square-pulses at 100 Hz (1 s duration; -14 V current amplitude).

COS-7 cell culture. COS-7 cells were grown in Dulbecco's Modified Eagle Medium (DMEM) without phenol-red (PAN Biotech, P04-01515) supplemented with 10% v/v foetal calf serum (FCS-Dominique Dutscher, 500105), 1% v/v penicillin/streptomycin (Dominique Dutscher, P06-07100) in 25 mL flasks (Falcon, 353082) at 37 °C, 5% CO_2. They were kept below 90% confluence, at which cells were washed in sterile filtered PBS (PAN Biotech, P04-36500), detached in a small volume of trypsin (PAN Biotech, P10-021100), washed in full warm medium and split 1/10 in a new flask. For imaging, 90% confluent cells were similarly detached with

trypsin and diluted 1/10 in full warm medium. COS7 cells were plated in uncoated petri dish. 24 hours after the plating, nanotubes were added (10 µl of the 3 mg/L PL-PEG nanotube solution and 60 µl of the 0.4 mg/L PL-PEG-NH_2 nanotube solution) to 1 mL of medium for 1h. The samples were rinsed 3 times for 5 minutes with medium and imaged under the fluorescent microscope.

Wide-field Fluorescence Microscopy Setup. Single SWCNT photoluminescence imaging was performed with an inverted microscope equipped with an electron-multiplying CCD camera (Princeton Instruments ProEm) and a 1.45 NA 60x objective in a wide-field geometry. The excitation source consisted of a tunable Ti:Sa laser emitting at a wavelength of 845 nm to preferentially excite (6,5) SWCNTs at the resonance of the dark K-momentum exciton[5]. The excitation intensity was kept at 10 kW/cm^2 with circularly polarized light. A dichroic mirror (FF875-Di01, Semrock) and a long-pass emission filter (ET900LP, Chroma) were used in order to illuminate and detect the SWCNT emitted fluorescence. Images of SWCNTs were recorded at 40 or 50 frames per second (typically 20,000 frames). GFP/Alexa488 (Excitation : FF02-472/30, Dichroic : FF495-Di03 and emission : FF01-520/35) and DAPI (Excitation : FF01-387/11, Dichroic : FF409-Di03 and emission : FF02-447/60) were imaged using epifluorescence white light excitation with appropriate filter sets.

Spinning disk microscope. Alexa568 imaging in acute slices was performed in a Leica DMI6000 inverted microscope (Leica Microsystems) with a Yokogawa spinning disk unit CSU-X1. The setup was equipped with live cell chamber and temperature was constantly kept at 37 °C. Tissue scans were obtained with either 10x air, 63x oil and 100x oil objectives, with exposure times of 50-100ms per frame. DAPI staining in fixed tissue was excited with a 405nm laser line, and detected through a standard DAPI emission filter. Images were acquired using an Evolve EM-CCD camera (Photometrics), setting the EM gain at 600.

NIR Spectrometer Setup. Emission spectra of single SWCNTs were collected using a cryogenically cooled 1D InGaAs detector (OMA V, Roper Scientific) placed at the output of a 150 mm spectrometer. A Chameleon (Coherent) pumped with a Ti:Sapphire laser (spectral range of 530-700 nm) and a Ti:Sa laser (spectral range of 700 to 850 nm) were used to generate a two-

dimensional photoluminescence excitation/emission map of the PL-PEG SWCNT solution. Individual spectra of the nanotube solution, in a 1 cm long quartz cuvette, were normalized by the incident power. The spectrum of a solution containing only surfactant, acquired under the same experimental condition, was subtracted for each laser wavelength. The proportion of nanotubes (6,5) in the solution was estimated by comparing the peak value for detected semi-conducting chiralities and assuming ~30% of metallic chiralities in HiPco samples.

Single cell loading. Single CA1 pyramidal neurons from 4-8 days in vitro (div) hippocampal organotypic slices were loaded with dilutions of carbon nanotubes to allow monitoring of their intracellular motion patterns. Briefly, nanotubes were dissolved (1/100 dilution) in a filtered cesium-based solution containing (in mM): 135 cesium-methanesulfonate, 8 NaCl, 10 HEPES, 0.2 EGTA, 4 Na_2ATP, 0.33 Na_3GTP, 5 tetraethylammonium chloride, pH 7.3 (all products from Sigma unless specified). This solution was supplemented with Alexa-488 (20 µg/mL) to allow further visual detection of the neurons of interest and used to fill 5-6 MΩ borosilicate patch pipettes. Single-cell loading was performed in 2 mL of pre-warmed (37°C / 5% CO_2) HEPES-based artificial cerebrospinal fluid (ACSF) containing (in mM): 130 NaCl, 2.5 KCl, 2.2 $CaCl_2$, 1.5 $MgCl_2$, 10 HEPES, 10 D-glucose. Nanotube transfer from the cesium-based solution to the cytoplasm was allowed by patching pyramidal neurons in whole-cell configuration.

Determination of SWCNT localization and orientation. Two-dimensional Gaussian functions with an arbitrary orientation were used to fit SWCNT images using homemade MatLab routines and determine SWCNT localizations (x_i, y_i), orientation θ_i, as well as large and small radii of the SWCNT image. Four consecutive images were averaged for each fit to improve localization precision (40 nm). SWCNT coordinates are then interconnected to reconstruct nanotube trajectories. When available, the positions of an immobile SWCNT was used to correct eventual small stage drifts over the 10 min recordings. Orientations ($\theta \in [0, \pi]$) obtained from the Gaussian fits are by construction doubly degenerate. The SWCNT orientation on the first image of the movie is assumed to be between $[0, \pi]$. This choice sets which end of the SWCNT is considered as the front of the tube. For all other orientations, continuity arguments are used to remove this degeneracy and to allow the orientation to be a real unbounded physical quantity ($\theta \in [-\infty, \infty]$).

Super-resolved images of the ECS from SWCNT localizations. For each trajectory, a super-resolved image of the ECS was computed by cumulating all SWCNT localizations (typically 20,000 points). In super-resolved images, each localization is displayed a two-dimensional Gaussian of 50 nm width and unit amplitude as commonly used in localization microscopy[6].

Estimation of SWCNT lengths. For each SWCNT trajectory imaged in live brain ECS, the distribution of eccentricity, obtained from the 2D asymmetric Gaussian fits of the nanotube images, was calculated when nanotube movements were undetectable (displacements between images < 40 nm). For each trajectory, the mean of the distribution was then used to determine the nanotube length (Figure S10) by comparison to the following model: the photoluminescence profile of a rigid nanotube of varying length L emitting at 986 nm was modelled as previously[7] using exciton diffusion length of ≈100 nm to provide a look-up table.

Atomic force microscopy (Figure S10b&c**).** PL-PEG SWCNTs were spin-coated on plasma-cleaned glass coverslips using a G3P-8 Spin coater (Specialty Coating Systems) at 930 rpm for 3 min. To remove excess PL-PEG, samples were rinsed using Milli-Q water. Atomic forced microscopy (AFM) images were recorded using an 8 nm diameter Si3N4 tip. For each well isolated SWCNT, the length was quantified using the NeuronJ plugin in ImageJ[8].

Mean squared displacements (MSD) analysis (Figure 2a). For each trajectory, three Mean Squared Displacement (MSD) curves were calculated as exemplified in Figure 2a: (i) MSD_{xy} in the laboratory frame corresponding to 2D movements in the imaging plane, and (ii) $MSD_{\parallel}$ and $MSD_{\perp}$ by decoupling 1D movements along ($\parallel$) and perpendicular ($\perp$) to the nanotube axis.

In order to decouple the diffusion of SWCNTs along and perpendicular to their principal axis, the displacement vector $(x_{i+1} - x_i, y_{i+1} - y_i)$ was determined at time t_{i+1} from the projection on the nanotube orientation vector obtained at time t_i (see inset of Figure 2a). This procedure to decouple the movements along and perpendicular to anisotropic object axis was presented previously[9-10]. One dimensional $MSD_{\parallel}$ and $MSD_{\perp}$could then be calculated from decoupled displacements (Figure 2a).

For one dimensional free diffusion, MSD curves are linear with time, with a slope equal to 2D. More precisely, $\mathrm{MSD}(\tau) = \langle \mathrm{r}^2 \rangle(\tau) = \int_{-\infty}^{+\infty} \mathrm{x}^2 \mathrm{c}(\mathrm{x}, \tau)\mathrm{dx} = 2\mathrm{D}\tau$, where D is the diffusion coefficient and $\mathrm{c}(\mathrm{x}, \mathrm{t})$ represents the probability of finding nanotubes at position x at time t if all nanotubes would be initially placed at x=0. $\mathrm{c}(\mathrm{x}, \mathrm{t})$ is the solution to the one dimensional diffusion equation $\frac{\partial \mathrm{c}(\mathrm{x},\mathrm{t})}{\partial \mathrm{t}} = \mathrm{D}\frac{\partial^2 \mathrm{c}(\mathrm{x},\mathrm{t})}{\partial \mathrm{x}^2}$ and equals $\mathrm{c}(\mathrm{x}, \mathrm{t}) = \frac{\mathrm{N}}{\sqrt{4\pi \mathrm{D}\mathrm{t}}} \mathrm{e}^{-\mathrm{x}^2/4\mathrm{D}\mathrm{t}}$, where N is the number of particles in the system.

Similarly, for two dimensional free diffusion, the MSD slope is equal to 4D since the MSD equals $\mathrm{MSD}(\tau) = \langle \mathrm{r}^2 \rangle(\tau) = \int_0^{+\infty} \rho^2 \mathrm{c}(\rho, \tau)\mathrm{d}\rho = 4\mathrm{D}\tau$ where $\mathrm{c}(\rho, \mathrm{t})$ is the solution of the two dimensional diffusion equation.

When the MSDs are not linear with time, a diffusion coefficient can be defined from the initial slopes of $\langle \mathrm{r}^2 \rangle(\tau)$ determined on short times.

Distribution of squared displacements (DSD) and calculation of $\langle \xi \rangle$ (Figures 2b-c, 4i and S11). Considering a diffusing particle, the cumulative distribution of squared displacements ($DSD^{\tau}(r^2)$) represents the probability of finding the particle at a distance less than r from its initial position after a time lag τ.

In the case of a freely diffusing particle along one coordinate, it is given by:

$$DSD^{\tau}(r^2) = \frac{\int_{-\mathrm{r}}^{+\mathrm{r}} \mathrm{c}(\mathrm{x},\tau)\mathrm{dx}}{\int_{-\infty}^{+\infty} \mathrm{c}(x,\tau)\mathrm{dx}} = \mathrm{erf}\left(\sqrt{r^2/4\mathrm{D}\tau}\right) = \mathrm{erf}\left(\sqrt{r^2/2\langle r^2 \rangle(\tau)}\right).$$

In the case of a mixture of particles following two distinct 1D diffusion behaviours (*e.g.* free diffusion with D_1 and D_2), the DSD is characterized summing two independent diffusive processes:

$$DSD^{\tau}(r^2) = \sum_{\mathrm{i}=1}^{2} \alpha_{\mathrm{i}} \cdot \mathrm{erf}\left(\sqrt{r^2/2\langle r^2 \rangle_i(\tau)}\right), \quad \text{(EQ1)}$$

where α_{i} are the fraction of particles in the different diffusive states (in the case of free diffusion : $\langle \mathrm{r}^2 \rangle_i(\tau) = 2\mathrm{D}_{\mathrm{i}}\tau$).

A similar analysis was previously used to retrieve different molecular populations bearing distinct 2D diffusion behaviours from the observation of many short trajectories[11-12].

Here a single and long trajectory of diffusing SWCNT displaying different temporal diffusive behaviours along its course is analysed. In order to retrieve the different diffusive

behaviours, the DSD analysis was performed on the displacements along and perpendicular to SWCNT axes.

From single trajectories, the cumulative distribution of squared displacement along each direction (parallel and perpendicular to the nanotube axis) was computed for every time lag (see examples in Figure S11 for the trajectory analysed in Figures 2 and 3). Each line corresponds to the experimental DSDs at a given time lag τ. Values of α_j and $\langle r^2 \rangle_j$ were estimated by fitting Equation EQ1 in each line. Two different diffusing processes were systematically retrieved from the global fitting procedure along each direction ($\langle {r_{\perp,\parallel}}^2 \rangle_{1,2}$). The evolutions $\langle {r_{\perp,\parallel}}^2 \rangle_{1,2}$ are presented in Figure S11C&D as a function of the time lag τ.

The evolution of $\langle {r_1}^2 \rangle_\perp$ is the slowest and displays a saturation revealing a confinement of the transverse movements of SWCNTs in the ECS. The typical ECS dimension responsible for this confinement can be estimated from the saturation value of $\langle {r_\perp}^2 \rangle_1$: $\langle \xi \rangle = \sqrt{6 \langle {r_\perp}^2 \rangle_1^{sat}}$[13].

Two-dimensional spatial maps of instantaneous diffusion coefficients and ECS local viscosity (Figures 3c, 4g&h and Extended Data movies 1 and 2). In order to create diffusion coefficient spatial maps, MSDs were calculated in the laboratory frame using a sliding window of 300 ms along each trajectory instead of the full trajectory as above. Linear fits of the initial slopes of the sliding MSDs were performed on the first 100 ms to obtain the instantaneous diffusion coefficients D_{xy} as a function of time. Values of instantaneous diffusion coefficients were obtained for each subset of detections ($t_0 - 150$ ms $\leq t \leq t_0 + 150$ ms) and associated to the centroid position (Figure 3c, 4e,g&h). Maps were created using pixels of 25 nm. Instantaneous diffusion coefficients falling within the same pixel were averaged. For visualization purposes, convolution with a two dimensional Gaussian of 50 nm FWHM was applied to smooth the data.

In order to link instantaneous diffusion coefficient values of the SWCNTs to local viscosities of the ECS, we used the relationship between the diffusion coefficient of highly anisotropic rods diffusing in a 2D plane and the viscosity[14] : $\eta = 3k_B T \ln(\phi) / (8\pi D_{xy} L)$. The nanotube length was estimated for each trajectory using the eccentricity of the imaged nanotube (see above).

Estimation of the ECS dimensions from the analysis of super-resolved images (Figure 3b and Figure S12). Super-resolved images revealed the diversity and complexity of the ECS morphology. In order to measure the typical dimensions of the ECS, we applied a global analysis by using a set of 2D Gaussian functions to directly fit the SWCNT localizations used to create the super-resolved images (Figure S12b). Initial guesses for applying Gaussian fitting was based on local density maxima of nanotube localizations (Figure S12a, inset & c). Two maxima that were closer than 75 nm could not induce two different Gaussian functions. The transverse dimensions of the set of 2D Gaussian functions used to fit the nanotube localizations provides the dimensions ξ of the ECS displayed in Figures 3b and S12a.

References for the Methods section:

1 Liu, Z. et al. In vivo biodistribution and highly efficient tumour targeting of carbon nanotubes in mice. Nat. Nanotechnol. 2, 47-52 (2007).

2 Gao, Z., Varela, J. A., Groc, L., Lounis, B. & Cognet, L. Toward the suppression of cellular toxicity from single-walled carbon nanotubes. Biomater. Sci. 4, 230-244 (2016).

3 Stoppini, L., Buchs, P. A. & Muller, D. A simple method for organotypic cultures of nervous tissue. J Neurosci Methods 37, 173-182 (1991).

4 Haas, K., Sin, W. C., Javaherian, A., Li, Z. & Cline, H. T. Single-cell electroporation for gene transfer in vivo. Neuron 29, 583-591 (2001).

5 Santos, S. M. et al. All-optical trion generation in single-walled carbon nanotubes. Phys. Rev. Lett. 107, 187401 (2011).

6 Godin, A. G., Lounis, B. & Cognet, L. Super-resolution microscopy approaches for live cell imaging. Biophys. J. 107, 1777-1784 (2014).

7 Oudjedi, L., Parra-Vasquez, A. N., Godin, A. G., Cognet, L. & Lounis, B. Metrological Investigation of the (6,5) Carbon Nanotube Absorption Cross Section. J. Phys. Chem. Lett. 4, 1460-1464 (2013).

8 Meijering, E. et al. Design and validation of a tool for neurite tracing and analysis in fluorescence microscopy images. Cytometry A 58, 167-176 (2004).

9 Han, Y. et al. Brownian motion of an ellipsoid. Science 314, 626-630 (2006).

10 Fakhri, N., MacKintosh, F. C., Lounis, B., Cognet, L. & Pasquali, M. Brownian motion of stiff filaments in a crowded environment. Science 330, 1804-1807 (2010).

11 Schutz, G. J., Schindler, H. & Schmidt, T. Single-molecule microscopy on model membranes reveals anomalous diffusion. Biophys. J. 73, 1073-1080 (1997).

12 Tardin, C., Cognet, L., Bats, C., Lounis, B. & Choquet, D. Direct imaging of lateral movements of AMPA receptors inside synapses. EMBO J. 22, 4656-4665 (2003).

13 Kusumi, A., Sako, Y. & Yamamoto, M. Confined lateral diffusion of membrane receptors as studied by single particle tracking (nanovid microscopy). Effects of calcium-induced differentiation in cultured epithelial cells. Biophys. J. 65, 2021-2040 (1993).

14 Han, Y., Alsayed, A., Nobili, M. & Yodh, A. G. Quasi-two-dimensional diffusion of single ellipsoids: aspect ratio and confinement effects. Phys Rev E Stat Nonlin Soft Matter Phys 80, 011403 (2009).

a

Brain extraction
and slice preparation

In vivo SWCNT
injection

b

Acute brain slice imaging

50 μm

60x
1.4 NA

845 nm

986 nm

c

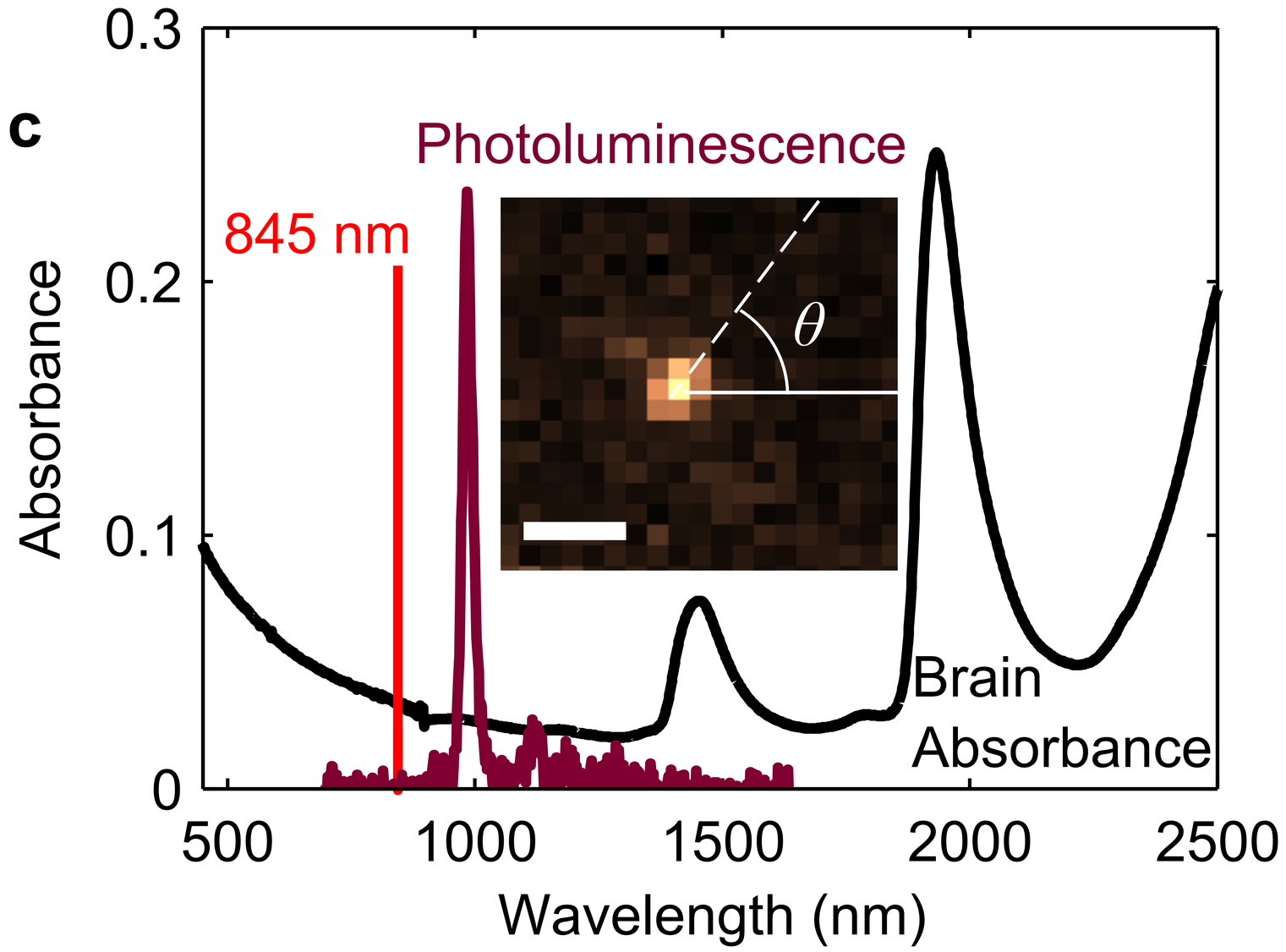

d

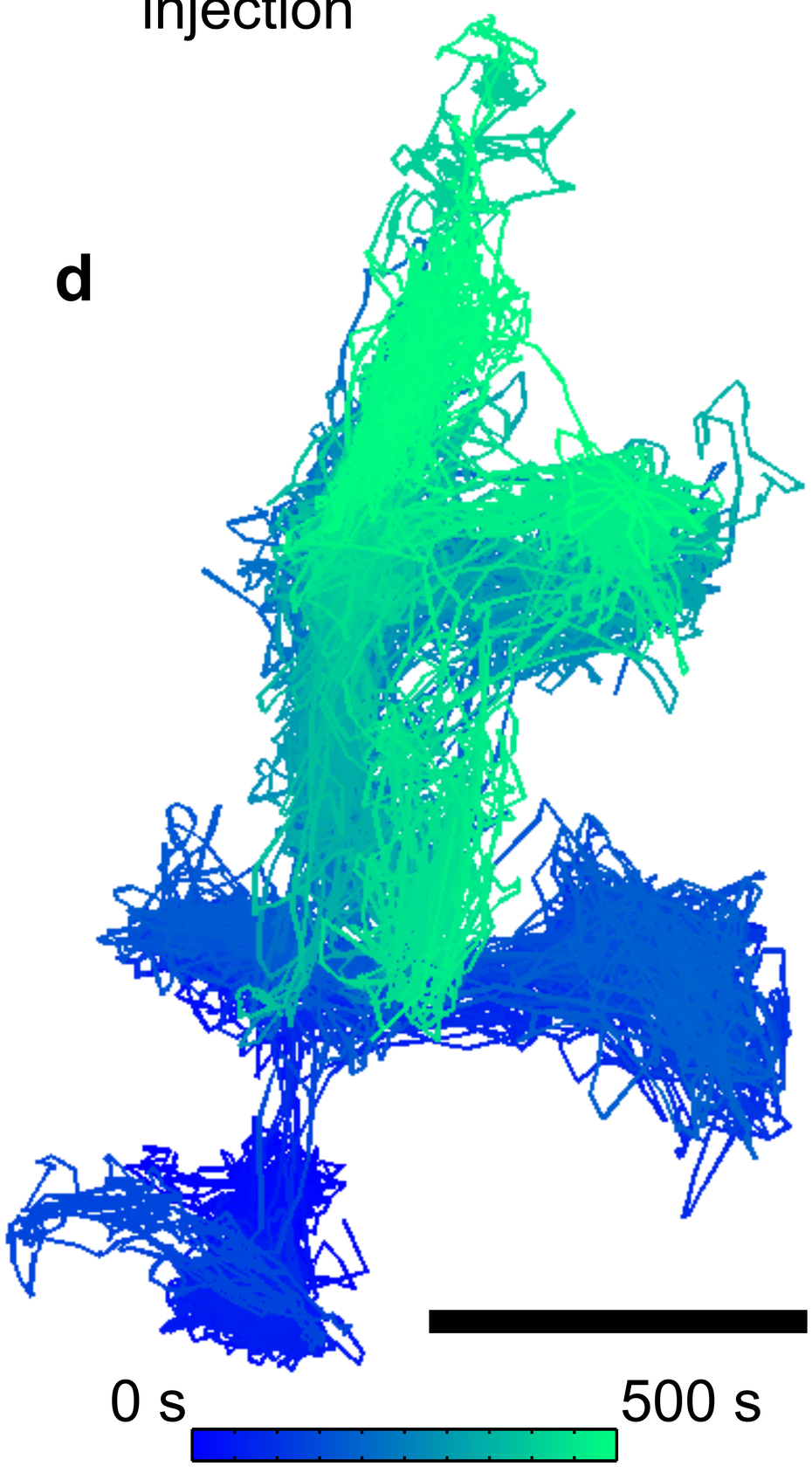

a

b

c

d

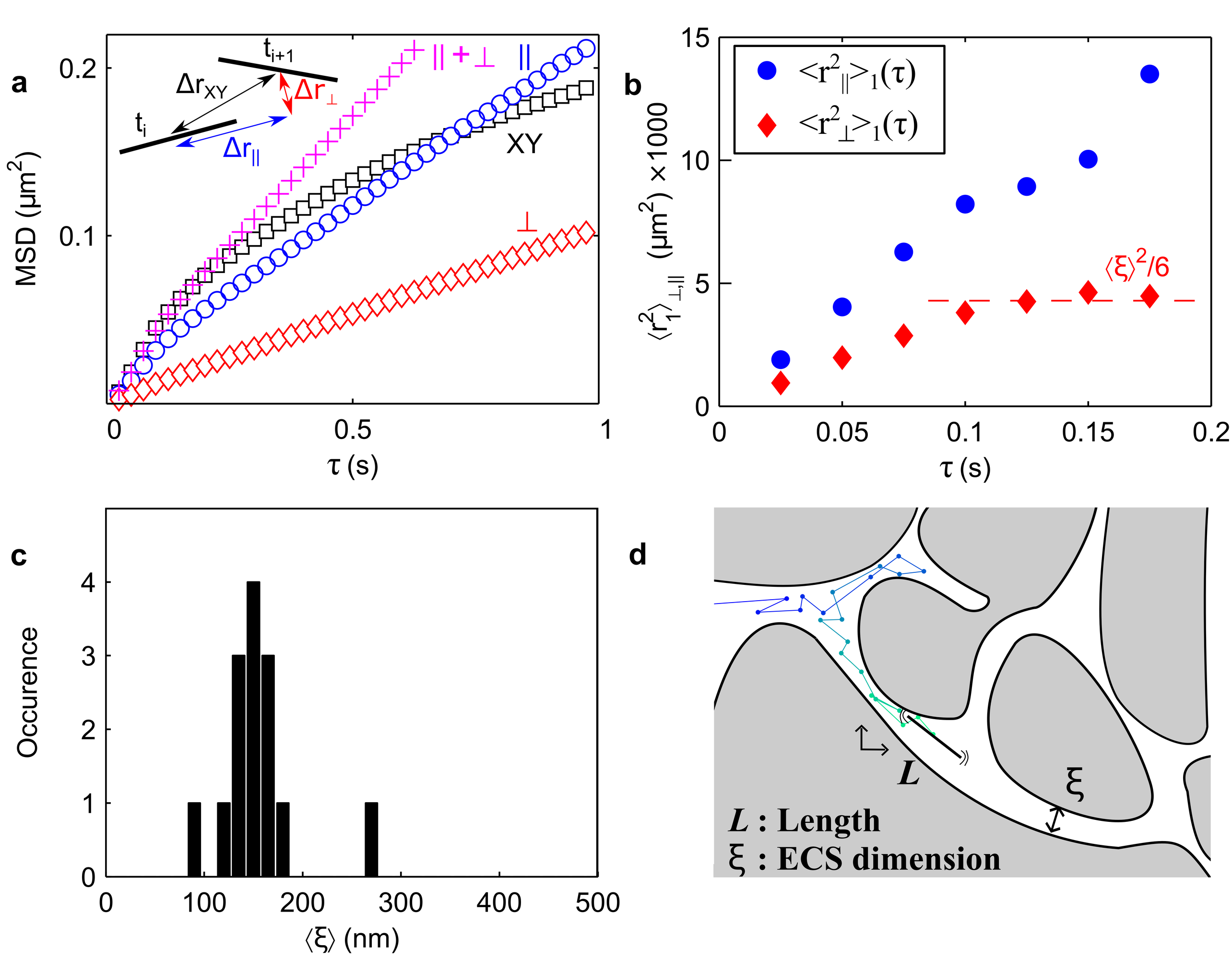
MSD (μm²)
0.2
0.1
0
0.5
1
τ (s)
t_{i+1}
t_i
Δr_XY
Δr_⊥
Δr_||
||
+
⊥
||
XY
⊥
<r²_||>₁(τ)
<r²_⊥>₁(τ)
⟨ξ⟩²/6
⟨r²₁⟩_⊥,|| (μm²) ×1000
15
10
5
0
0.05
0.1
0.15
0.2
τ (s)
Occurence
4
3
2
1
0
100
200
300
400
500
⟨ξ⟩ (nm)
L
ξ
L : Length
ξ : ECS dimension

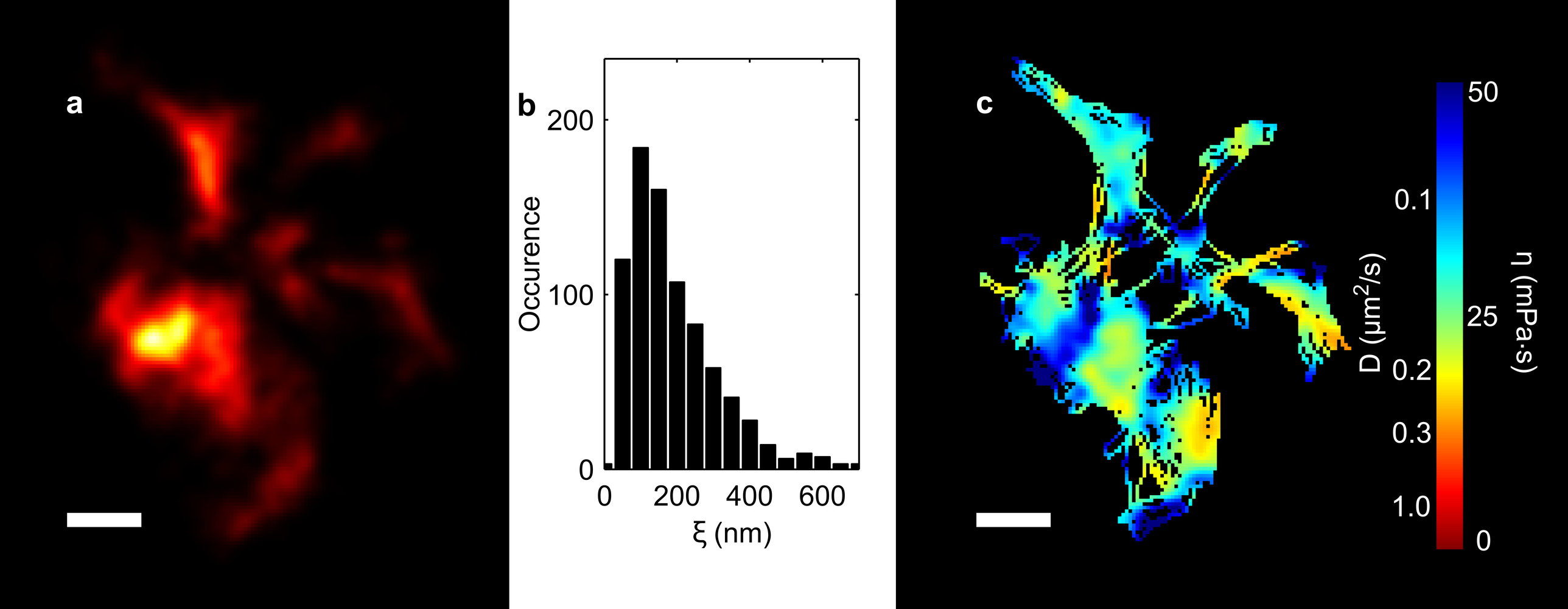
a
b
200
100
0
Occurence
0
200
400
600
ξ (nm)
c
50
0.1
25
0.2
0.3
1.0
0
D (μm²/s)
η (mPa·s)

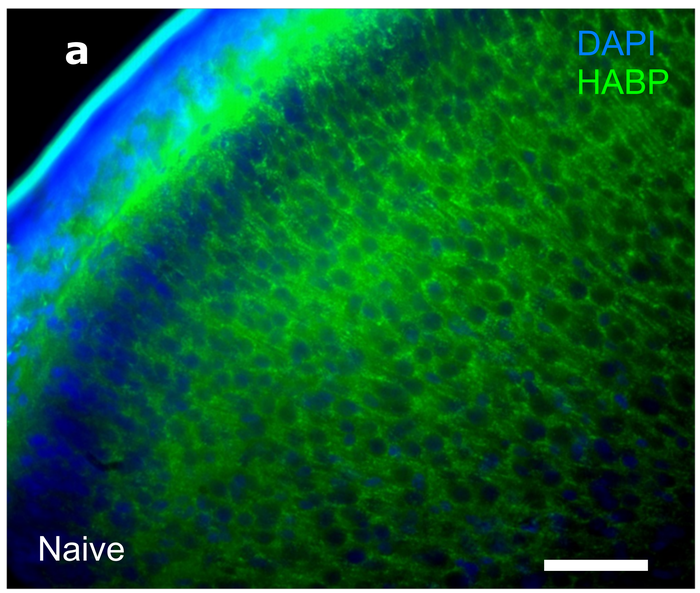
a
DAPI
HABP
Naive

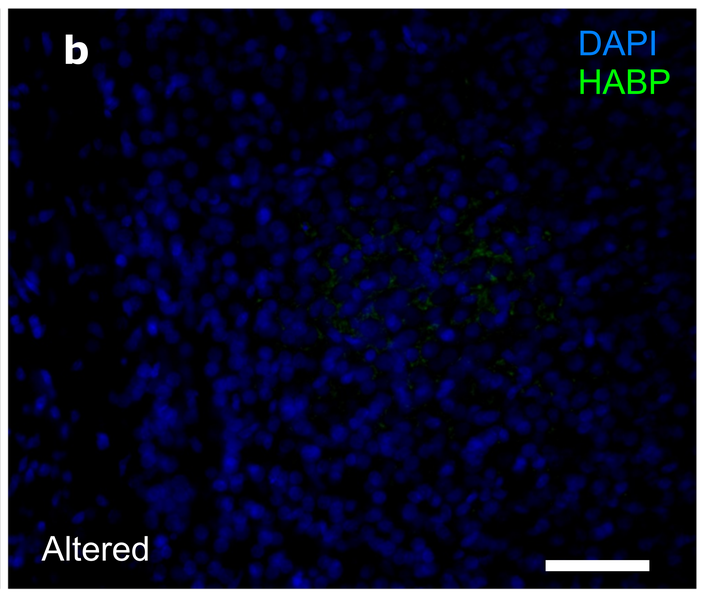
b
DAPI
HABP
Altered

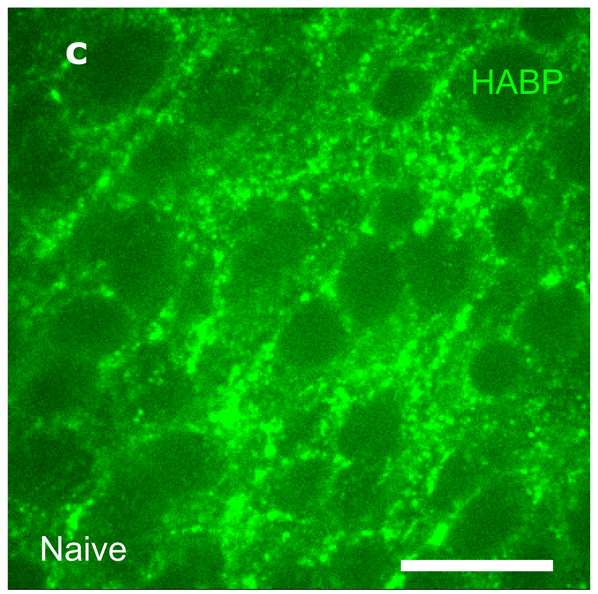
c
HABP
Naive

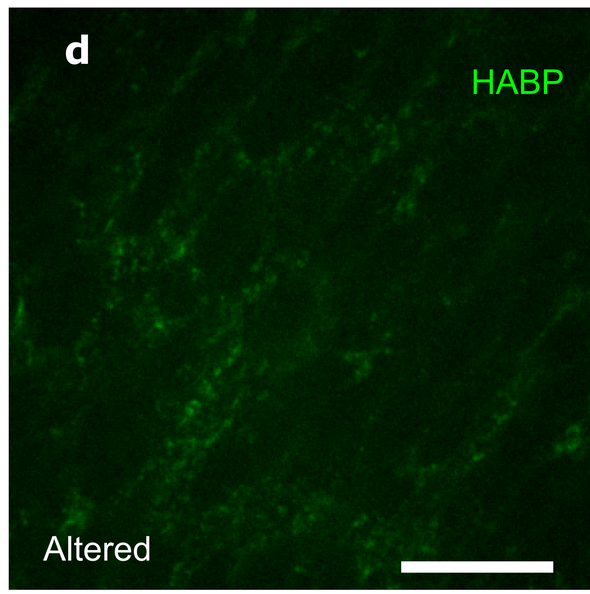
d
HABP
Altered

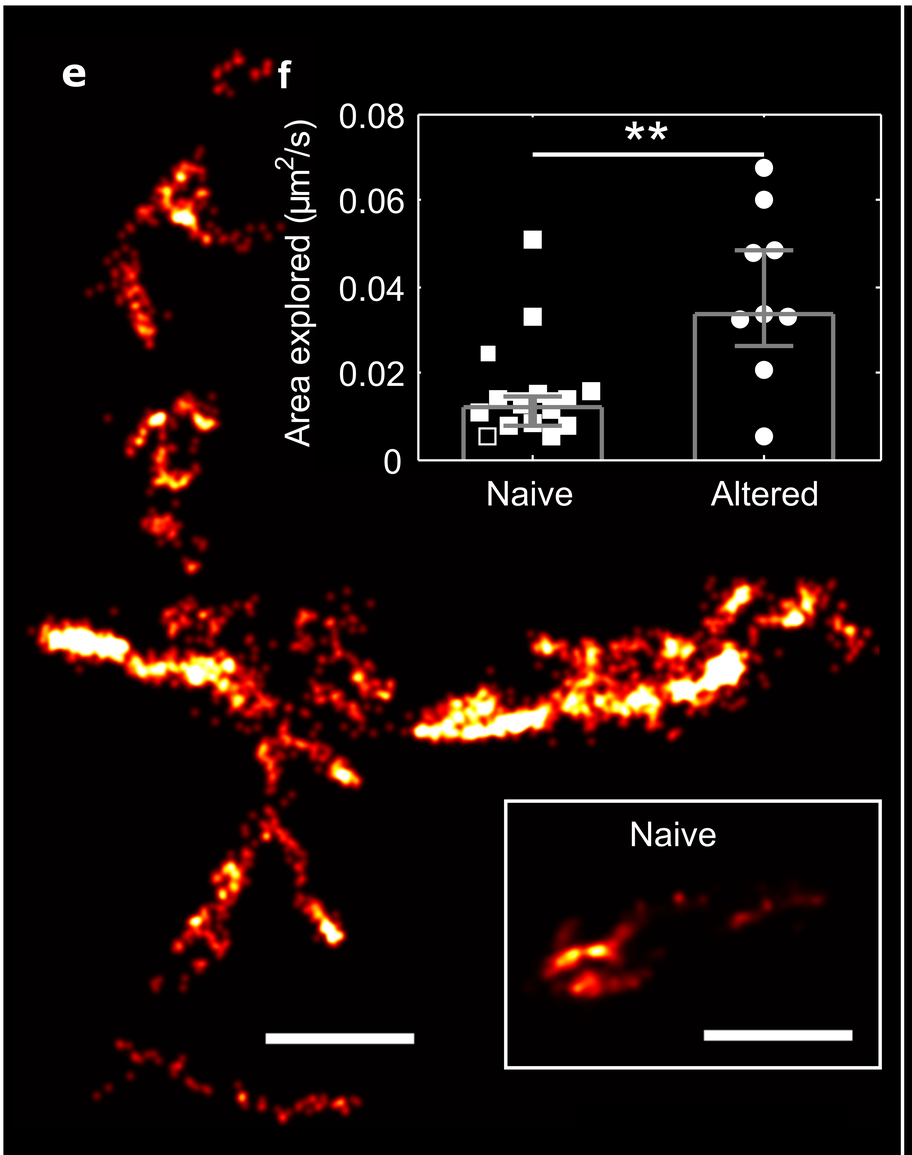
e
Naive
Altered

f
Area explored (μm²/s)
0.08
0.06
0.04
0.02
0
**
Naive
Altered

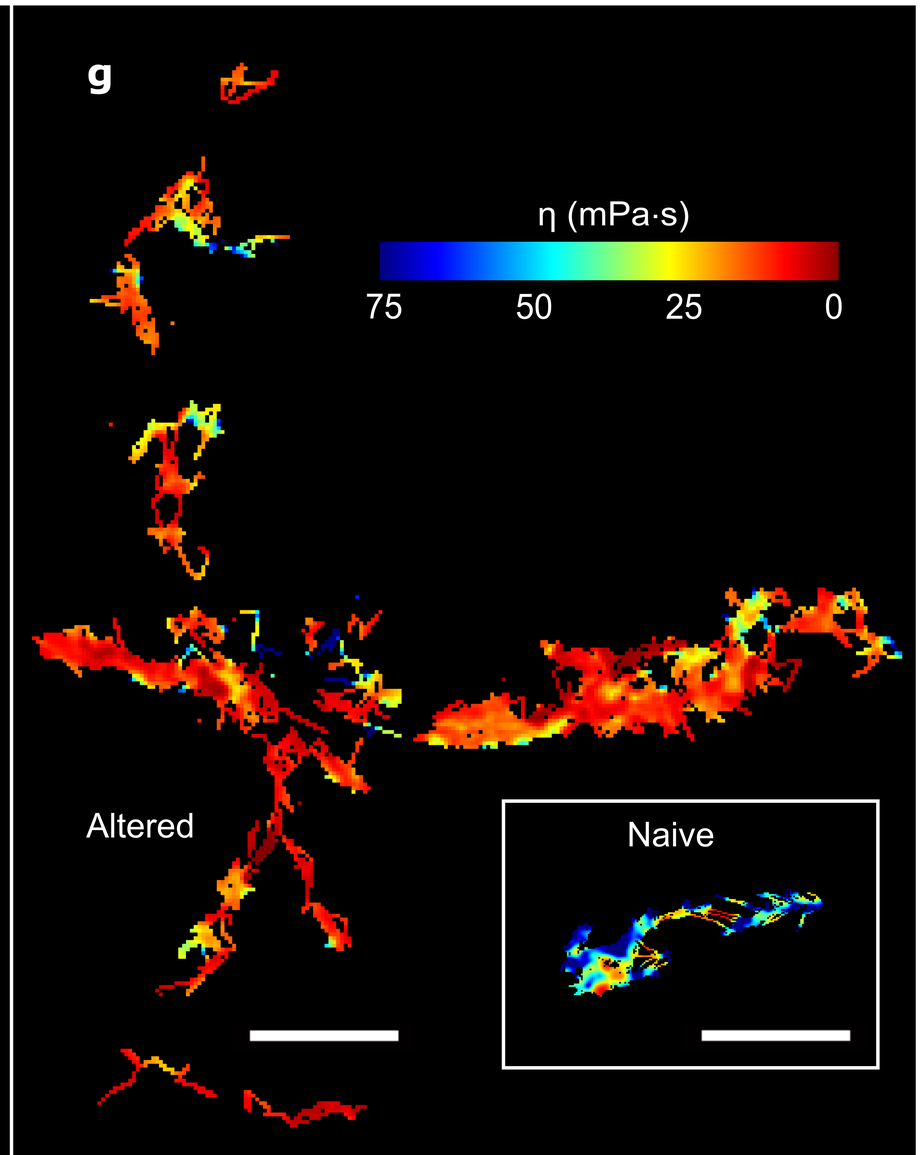
g
η (mPa·s)
75
50
25
0
Altered
Naive

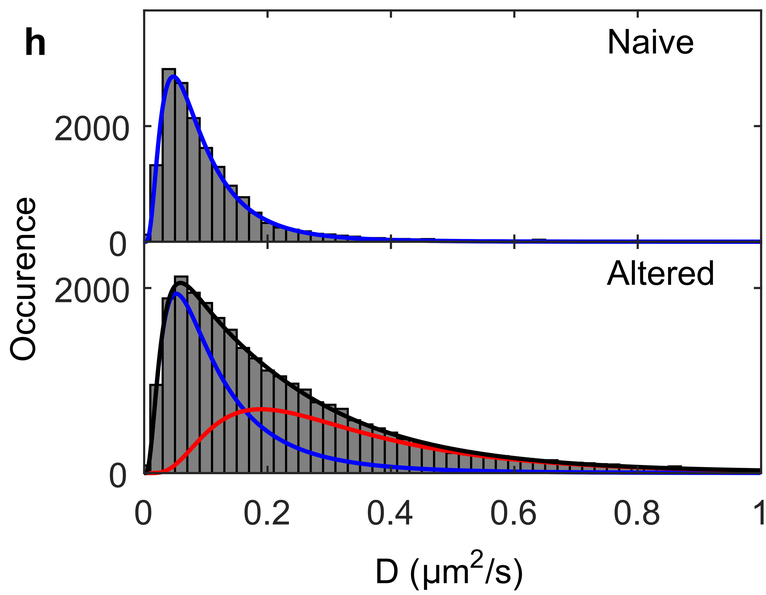
h
Naive
Altered
Occurence
2000
0
2000
0
0
0.2
0.4
0.6
0.8
D (μm²/s)

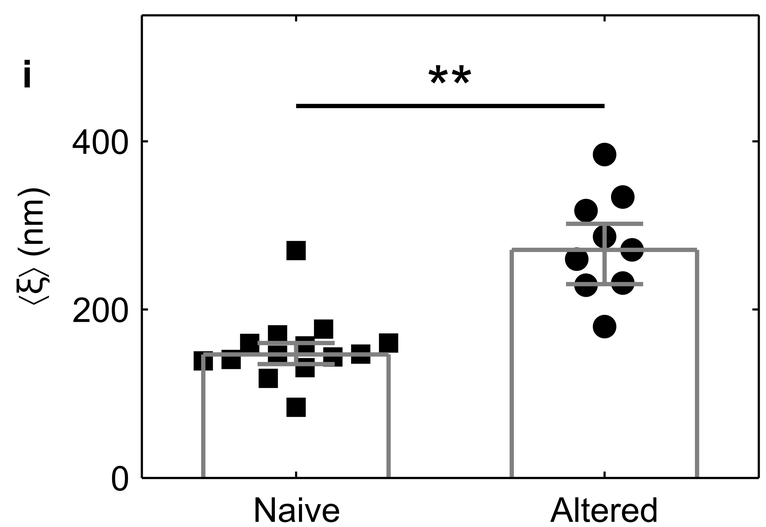
i
**
⟨ξ⟩ (nm)
400
200
0
Naive
Altered